# Dynamics of the $s = \frac{1}{2}$ linear Heisenberg antiferromagnet in a magnetic field: Experiment and theory

J. P. Groen, T. O. Klaassen, and N. J. Poulis
*Kamelingh Onnes Laboratorium der Rijksuniversiteit Leiden, Leiden, The Netherlands*

G. Müller and H. Thomas
*Institut für Physik der Universität Basel, CH-4056 Basel, Switzerland*

H. Beck
*Institut de Physique de l'Université de Neuchâtel, CH-2000 Neuchâtel, Switzerland*

(Received 3 March 1980)

Proton spin-lattice relaxation times have been measured in the quasi-one-dimensional $s = \frac{1}{2}$ Heisenberg antiferromagnetic compounds $CuSeO_4 \cdot 5H_2O$ and $CuSO_4 \cdot 5H_2O$, in order to study the magnetic field dependence of the 1D quantum spin dynamics at various temperatures. Information is obtained on the low-frequency behavior of the spin autocorrelation functions for the linear chains. The transverse component shows at high $T$ a marked decrease with magnetic field above the saturation field $B_c$. Towards lower temperatures a pronounced maximum just below $B_c$ develops and the decrease above $B_c$ becomes more abrupt. The longitudinal component behaves more smoothly near and above $B_c$. The field dependence of the relaxation rates is well explained at all nonzero temperatures by finite-chain calculations. For $T = 0$ we present analytical calculations of autocorrelation functions based on the predominance of a two-parameter spin-wave continuum for the quantum spin dynamics yielding a nondivergent behavior at $\omega = 0$ and $B = 0$. Exact results are obtained for fields above $B_c$. Further, an effective $XY$ approach is used for low but finite $T$. Here, good agreement is found with the proton relaxation data for very low temperatures.

## I. INTRODUCTION

The dynamical behavior of antiferromagnetic linear chains has become an important subject of experimental as well as theoretical studies. Experimental information has been obtained by neutron diffraction,[1,2] electron-spin resonance,[3] frequency-dependent susceptibility measurements,[4] and nuclear magnetic resonance.[5,6] Most attention has been paid to the low-field and high-temperature region. In most cases the results could be understood by classical theories. For more recent experiments on $s = \frac{1}{2}$ systems at low temperatures, classical theories fail to explain the results.[2,7,8] Obviously, the quantum-mechanical nature of the system has to be taken into account here. However, exact theoretical results for the low-temperature dynamics of the quantum chain are more or less restricted to the $XY$ model.[9–11] A detailed understanding of the linear $s = \frac{1}{2}$ Heisenberg antiferromagnet (HB AF) in a magnetic field has been obtained by a recent approach which takes the effect of a two-parameter spin-wave continuum for the quantum spin dynamics into account.[12–14] Recent NMR $T_1$ measurements at very low temperatures have been explained by a quantum-mechanical approach based on the $XY$ model and the Bulaevskii approximation for the HB AF.[8] Similar results have recently been obtained by Azevedo *et al.*[15] and were interpreted in boson and fermion pictures.

NMR experiments can be used to obtain information on the low-frequency dynamics at low temperatures where quantum effects are expected to be important and in high magnetic fields. The crystals $CuSeO_4 \cdot 5H_2O$ and $CuSO_4 \cdot 5H_2O$ are good candidates for this purpose, since, due to their convenient value of the exchange interaction, high reduced fields and low relative temperatures can be reached at the same time. Besides, the static properties of these compounds have been studied extensively.[16]

Finite-chain calculations have provided quantitative results for static properties[17,18] and for high-temperature dynamic properties,[19] as well as more qualitative results for the low-temperature dynamics.[20,21] In this paper we show that such finite-chain calculations give results even at relatively low temperatures, which are in quantitative agreement with NMR experimental data and with other theoretical approaches such as $T = 0$ analytic calculations and a finite-temperature effective $XY$ approximation. For very low temperatures, the critical behavior near the

 

saturation field becomes important. Here, the NMR $T_1$ results are best interpreted by a $T=0$ analytic approach. The results show considerable deviations from the behavior of a classical antiferromagnetic chain, due to the quantum nature of the system. We mention here especially the result that the spin autocorrelation function at $\omega=0$, $B=0$ shows no divergence for $T\to 0$ in contrast to the classical case.[5,22] This is due to the effect of a two-parameter spin-wave continuum present in the quantum HB AF which is quite different from the spin-wave structure of a classical model.

In Sec. II we review the properties of the crystals $CuSO_4\cdot 5H_2O$ and $CuSeO_4\cdot 5H_2O$, and discuss the interpretation of proton relaxation in terms of spin-correlation functions for the magnetic linear chain. In Sec. III the experimental results for the angular dependence of the relaxation rates are analyzed, and it is shown how separate information can be obtained on the longitudinal and transverse autocorrelation functions. Section IV describes the evaluation of autocorrelation functions by finite-chain calculations, and presents the predictions of these calculations as well as a $T=0$ analytic approach and a $T>0$ effective $XY$ treatment for the dynamics in a magnetic field. In Sec. V comparison is made between experiment and theory.

## II. PROTON RELAXATION IN $CuSO_4\cdot 5H_2O$ AND $CuSeO_4\cdot 5H_2O$

The crystals $CuSO_4\cdot 5H_2O$ and $CuSeO_4\cdot 5H_2O$ contain two types of magnetic ions. The copper ions at the 000 sites are coupled into antiferromagnetic Heisenberg linear chains with effective spin quantum number $s=\frac{1}{2}$ and with exchange constants $J/k_B=1.45$ K for $CuSO_4\cdot 5H_2O$ and $J/k_B=0.85$ K for $CuSeO_4\cdot 5H_2O$.[23] The copper ions at the $\frac{1}{2}\,\frac{1}{2}0$ position in the unit cell have relatively small interaction with each other, characterized by Curie-Weiss temperatures of the order of 0.05 K. The transition to a three dimensionally ordered phase has been found to occur at 100 mK for the sulphate and at 125 mK for the selenate.[24] This indicates that the interchain couplings are relatively small. The interaction $J_{12}$ of a linear-chain spin with its $z_{12}$ neighboring "paramagnetic" spins has been determined to be $z_{12}J_{12}/k_B\simeq -0.2$ K (ferromagnetic). The unit cell contains 10 nonequivalent protons, leading to 10 distinct NMR lines. For more information about the crystal structure, the identification of the different protons, and the magnetic properties, we refer to Ref. 25 and references therein. In earlier work, NMR has been used extensively to study the static magnetic behavior of linear-chain systems, and some information on the dynamics has been obtained by measuring relaxation times of proton spins.[8,25,26]

The longitudinal proton spin relaxation rate $T_{1n}^{-1}$ in concentrated magnetic crystals can be expressed in terms of time-dependent correlation functions for the copper spins in the crystal.[27] For an isotropic (Heisenberg) electron-spin system with a uniform field $B$ in the $z$ direction, the result is

$$T_{1n}^{-1}=\sum_{ij}\left[a_{ij}\phi_{j-i}^{z}(\omega_n)+b_{ij}\phi_{j-i}^{+}(\omega_n)\right] . \tag{2.1}$$

Here $\phi_{j-i}^{z}(\omega_n)$ and $\phi_{j-i}^{+}(\omega_n)$ are Fourier transforms of the two-spin correlation functions

$$\phi_{j-i}^{z}(\omega)=\int_{-\infty}^{+\infty}dt\,\langle\delta S_i^z(t)\delta S_j^z(0)\rangle\cos\omega t , \tag{2.2}$$

$$\delta S_i^z(t)=S_i^z(t)-\langle S_i^z\rangle ,$$

$$\phi_{j-i}^{+}(\omega)=\tfrac{1}{2}\int_{-\infty}^{+\infty}dt\left[\langle S_i^+(t)S_j^-(0)\rangle e^{i\omega t}+\langle S_i^-(t)S_j^+(0)\rangle e^{-i\omega t}\right] , \tag{2.3}$$

at the nuclear Larmor frequency $\omega=\omega_n$ of the proton spins. The coefficients $a_{ij}$ and $b_{ij}$ are related to the magnetic interactions of the nuclear spin under consideration with electron spins $i$ and $j$.

In this paper we present relaxation measurements on proton 3 (Ref. 25) of $CuSO_4\cdot 5H_2O$ and $CuSeO_4\cdot 5H_2O$. This proton interacts strongly with the nearest electron spin of the linear-chain system and more weakly with the nearest "paramagnetic" spin. The interactions with all other electron spins are calculated to be considerably smaller, and their contributions to the relaxation rate will be disregarded. Assuming further that the pair correlations between the two nearest spins do not contribute significantly, we take only the autocorrelation ($i=j$) contributions of these electron spins into account:

$$T_{1n}^{-1}=a_{00}\phi_0^z(\omega_n)+b_{00}\phi_0^+(\omega_n)+a_p\phi_p^z(\omega_n) . \tag{2.4}$$

Here we have used the experimental results of Henkens that for the paramagnetic system at nonzero fields $\phi_p^+(\omega_n)\approx 0$.[25] The term $\phi_p^z(\omega_n)$ can be estimated from measurements of the relaxation rate of a proton near the paramagnetic system.[25]

If the interaction between electron spins and proton spins can be described as a combination of point-dipolar interaction and an isotropic superhyperfine interaction $A$, the coefficients $a_{00}$ and $b_{00}$ in Eq. (2.4) are given by

$$a_{00}=\left(\frac{\mu_0}{4\pi}\right)^2\frac{\gamma_e^2\gamma_n^2\hbar^2}{r^6}\frac{9}{2}\sin^2\theta\cos^2\theta , \tag{2.5}$$

$$b_{00}=\left(\frac{\mu_0}{4\pi}\right)^2\frac{\gamma_e^2\gamma_n^2\hbar^2}{r^6}\left[\tfrac{1}{8}(1+x-3\cos^2\theta)^2+\tfrac{9}{8}\sin^4\theta\right] , \tag{2.6}$$

where

$$x=2A\left(\frac{\mu_0}{4\pi}\frac{\gamma_e\gamma_n\hbar}{r^3}\right)^{-1} . \tag{2.7}$$

The expression for $a_p$ is similar to that for $a_{00}$. In Eqs. (2.5) and (2.6) $r$ is the length of the vector $\vec{r}$ pointing from the proton to the electron spin, and $\theta$ is the angle between $\vec{r}$ and the field direction $z$. For an electron-spin system with isotropic interactions, the quantities $\phi_0^z(\omega_n)$, $\phi_0^+(\omega_n)$, and $\phi_p^z(\omega_n)$ do not depend on the direction of the field, which means that the angular dependence of the relaxation rate is only due to $a_{00}$, $b_{00}$, and $a_p$.

For comparison with theory we introduce here the quantities obtained theoretically (see Sec. IV)

$$F^{\mu\nu}(\omega)=\int_{-\infty}^{+\infty} dt\,\langle \delta S_i^{\mu}(t)\delta S_i^{\nu}(0)\rangle e^{i\omega t}\ , \qquad (2.8)$$

with $\mu, \nu = x,y,z,+$, or $-$. These autocorrelation functions are related to the ($j=0$) functions of Eqs. (2.2) and (2.3) by

$$\phi_0^z(\omega_n)=\tfrac{1}{2}(1+e^{-\beta\hbar\omega_n})F^{zz}(\omega_n)\ , \qquad (2.9)$$

$$\phi_0^+(\omega_n)=\tfrac{1}{2}[F^{+-}(\omega_n)+F^{-+}(-\omega_n)]\ . \qquad (2.10)$$

Since the nuclear Larmor frequency $\omega_n$ is small compared to the exchange constant (which is our unit of energy in the theoretical part) even at the highest fields used, we consider the zero-frequency limit in all theoretical quantities. Moreover, $\beta\hbar\omega_n$ is still small even at the highest fields and the lowest temperatures used in the experiments, such that $\exp(-\beta\hbar\omega_n)\approx 1$ in Eq. (2.9). In order to obtain the zero-temperature behavior, one has, of course, to be careful to take the correct limit $\lim_{\omega\to 0}\lim_{T\to 0}$.

## III. EXPERIMENTAL RESULTS

Longitudinal proton spin relaxation times $T_{1n}$ have been obtained with a noncoherent spin-echo apparatus, consisting of a pulsed power oscillator and a receiver. The pulse program consisted of a saturating pulse, followed by a 90°–180° pulse set to produce the echo, which monitors the $z$ component of the nuclear magnetization. The relaxation was found to be exponential over at least 1.5 decades.

The measurements were performed with the sample in a liquid $^4$He bath and for temperatures below 1.2 K in a $^3$He cryostat. The required magnetic fields were generated with homogeneous superconducting magnets. For the $^4$He temperature measurements, the crystal could be rotated with respect to the field, produced by a superconducting solenoid. For the $^3$He measurements, a split coil magnet was used,[28] which could be rotated with respect to the crystal.

The relaxation times have been obtained on single crystals of $CuSO_4\cdot 5H_2O$ and $CuSeO_4\cdot 5H_2O$. The measurements were performed on single resonance lines that were well separated from the other lines. Therefore, the predicted angular dependence according to Eqs. (2.5) and (2.6) could be observed directly. As expected, the angular dependence of the relaxation rate of a proton near a "paramagnetic" ion (proton 1) has the characteristic $\sin^2\theta_p\cos^2\theta_p$ angular dependence of $a_p$. The completely different angular dependence of $T_{1n}^{-1}$ for proton 3 (near a linear-chain ion) in low fields directly displays the presence of the $\phi_0^+(\omega_n)$ contribution.

In Figs. 1 to 4 we present experimental results for the relaxation rate of proton 3 in $CuSO_4\cdot 5H_2O$ as a function of the field direction in the plane perpendicular to the crystallographic $c$ axis. The angle $\phi$ in the figures is related to $\theta$ in Eqs. (2.5) and (2.6) through

$$\cos\theta=\cos\theta_0\cos(\phi-\phi_0)\ . \qquad (3.1)$$

From the crystal structure[29] one finds that the angle of the copper-proton line with the plane perpendicular to $c$ is $\theta_0\approx 3.5°$ and that $\phi_0\approx 43.5°$. The analogous quantities for the nearest paramagnetic ion and proton 3 are $\theta_{p0}\approx 6.1°$ and $\phi_{p0}\approx 21.3°$.

According to the measurements on a proton near an ion of the paramagnetic system (proton 1), the field and temperature dependence of the contribution from the paramagnetic system is expected to be approximately proportional to $1-m^2(B,T)$, where $m(B,T)$ is the reduced magnetization of the paramagnetic system. This is similar to the result of Henkens.[25] The proportionality constant for proton 3 has been adjusted to obtain a reasonable fit in high magnetic fields (Figs. 1 and 2). The value of the proportionality constant obtained in this way is 30% smaller than calculated from the relaxation rate of proton 1 on the basis of point-dipolar electron-proton interaction. In each of the figures the contribution to the relaxation rate of proton 3 obtained from the nearest paramagnetic electron spin is given by the dotted line. The contributions from the linear-chain system were fitted separately in each figure by adjusting the magnitude of $\phi_0^+(\omega_n)$ and $\phi_0^z(\omega_n)$. From the experimental results near $\theta=90°$ and $\theta=0°$ ($\phi\approx 125°$ and $\phi\approx 35°$) the $\phi_0^+(\omega_n)$ contribution can be deduced, since for these directions $a_{00}$ is small or zero. $\phi_0^+(\omega_n)$ is found to be very small for high fields (Figs. 1 and 2) but large below the saturation field $B_c=4J/g\mu_B\approx 3.8T$ (Figs. 3 and 4). The dot-dashed lines in the latter two figures represent this contribution. In agreement with earlier work[8] the parameter $x$ in Eq. (2.6) has been taken equal to $-0.45$. To complete the analysis of the angular dependence of $T_{1n}^{-1}$, the magnitude of the $\phi_0^z(\omega_n)$ contributions (dashed lines) has been adjusted to obtain the best overall fit. The resulting total relaxation rates are given by the solid lines.

In Figs. 1 to 4 it is seen that the point-dipolar model gives a reasonable explanation of the angular dependence of the relaxation rate. In a previous paper[8] it has been shown that the data for $T=0.5$ K for $CuSO_4\cdot 5H_2O$ fit well within this description. The deviations are somewhat larger for the results at higher

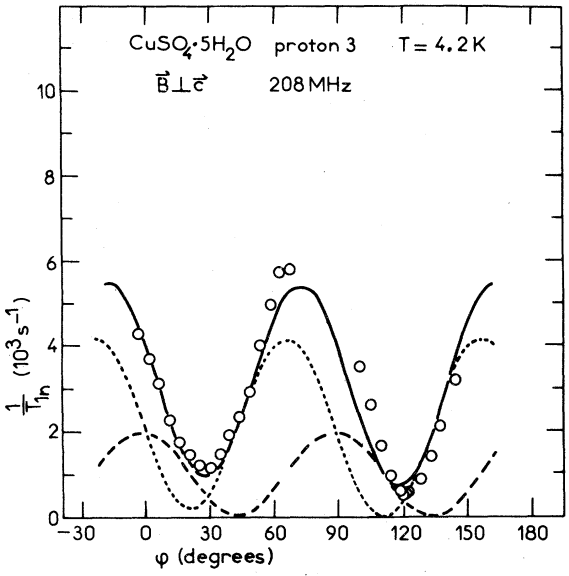


FIG. 1. Dependence of the relaxation rate of proton 3 in $CuSO_4 \cdot 5H_2O$ on the direction of the field for $B > B_c$ at 4.2 K. The solid line represents the result of a fit of Eq. (2.4) to the data, with contributions from $\phi_0^z(\omega_n)$ (dashed line) and $\phi_p^z(\omega_n)$ (dotted line).

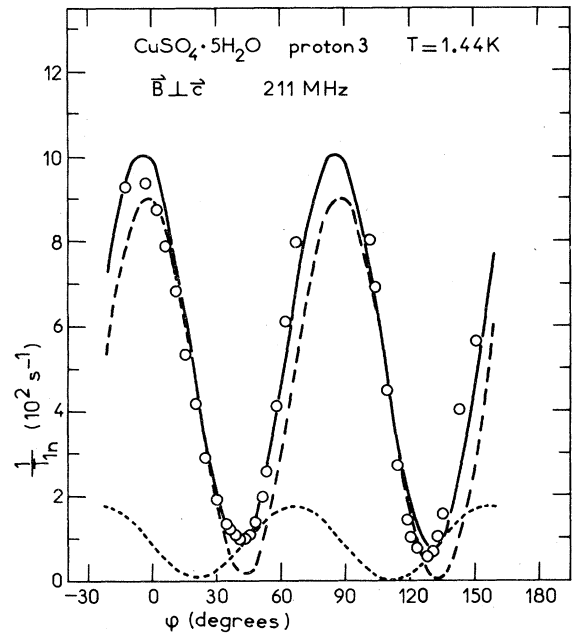


FIG. 2. Dependence of the relaxation rate of proton 3 in $CuSO_4 \cdot 5H_2O$ on the direction of the field for $B > B_c$ at 1.44 K. The solid line represents the result of a fit of Eq. (2.4) to the data, with contributions from $\phi_0^z(\omega_n)$ (dashed line) and $\phi_p^z(\omega_n)$ (dotted line).

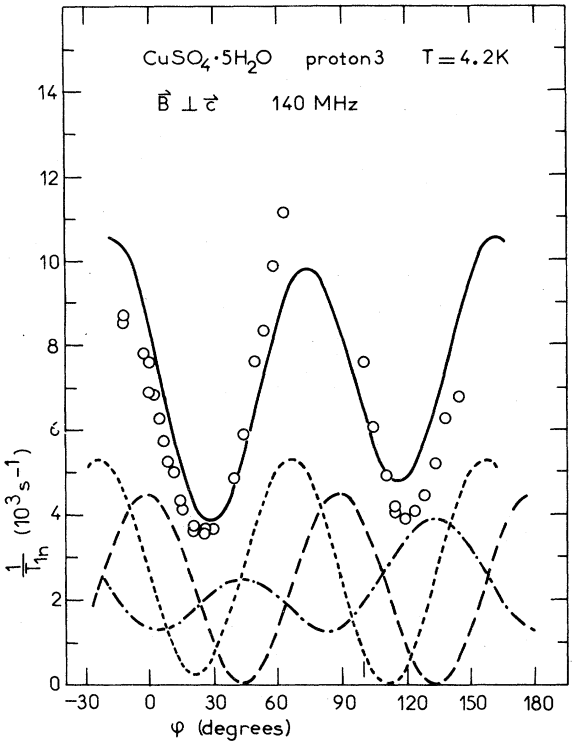


FIG. 3. Dependence of the relaxation rate of proton 3 in $CuSO_4 \cdot 5H_2O$ on the direction of the field for $B < B_c$ at 4.2 K. The solid line represents the result of a fit of Eq. (2.4) to the data, with contributions from $\phi_0^z(\omega_n)$ (dashed line), $\phi_p^z(\omega_n)$ (dotted line), and $\phi_0^+(\omega_n)$ (dot-dashed line).

temperatures, especially for 4.2 K below $B_c$. However, since several approximations have been made, these deviations are not too surprising. Deviations from point-dipolar interaction and effects from the anisotropic $\overleftrightarrow{g}$ tensor will lead to a somewhat different angular dependence. Also the neglect of contributions from other than the two nearest Cu ions may introduce a small discrepancy. Contributions due to other magnetic ions are estimated to give corrections of the order of 10% to the relaxation rate, mainly due to the nearest-neighbor pair-correlation functions of the linear-chain system.

From the angular dependence it is clear that the relaxation rate near $\phi \approx 125°$ ($\theta \approx 90°$) is predominantly determined by $\phi_0^+(\omega_n)$. Measurements of the field and temperature dependence for this field direction provides therefore direct information about $\phi_0^+(\omega_n)$. For the highest temperature, contributions from $\phi_p^z(\omega_n)$ and $\phi_0^z(\omega_n)$ are expected to be not completely negligible (see Figs. 1 and 3). The description of the angular dependence is, however, not accurate enough to correct the results for these small contributions. Information on $\phi_0^z(\omega_n)$ can be obtained by measurements in field directions where $a_{00}$ is large.

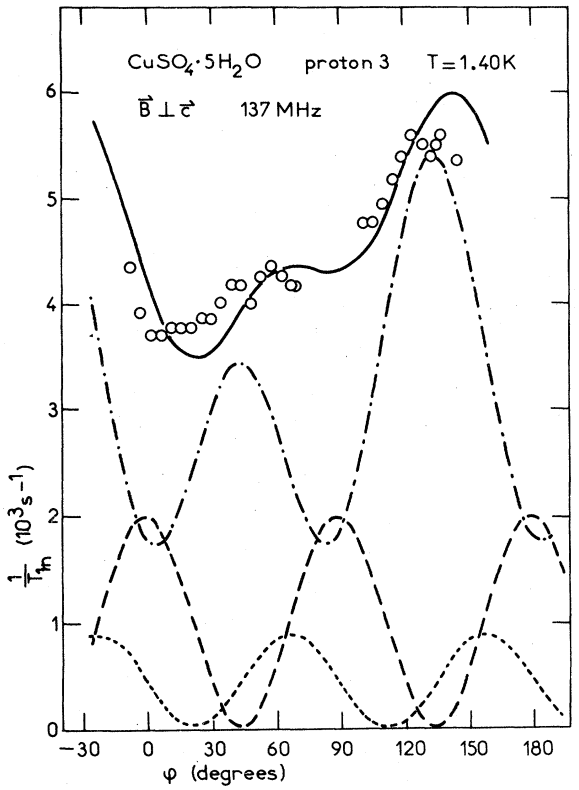


FIG. 4. Dependence of the relaxation rate of proton 3 in $CuSO_4 \cdot 5H_2O$ on the direction of the field for $B < B_c$ at 1.40 K. The solid line represents the result of a fit of Eq. (2.4) to the data, with contributions from $\phi_0^x(\omega_n)$ (dashed line), $\phi_p^z(\omega_n)$ (dotted line), and $\phi_0^+(\omega_n)$ (dot-dashed line).

However, there is always also a large contribution of $\phi_0^+(\omega_n)$ present, which has to be subtracted. Further corrections have to be made for the $\phi_p^z(\omega_n)$ contributions. This makes it difficult to obtain results for $\phi_0^x(\omega_n)$ as reliable as for $\phi_0^+(\omega_n)$, except for the lowest temperatures and fields above the critical field, where both $\phi_0^+(\omega_n)$ and $\phi_p^z(\omega_n)$ may be neglected. For a suitable field direction, direct results can be obtained for $\phi_0^x(\omega_n)$ there. Results for the field dependence of $\phi_0^+(\omega_n)$ at various temperatures and some results for $\phi_0^x(\omega_n)$ are presented in Sec. V.

## IV. AUTOCORRELATION FUNCTIONS FOR THE $s=\frac{1}{2}$ HEISENBERG ANTIFERROMAGNETIC CHAIN

Here we study the dynamics of the one-dimensional isotropic $s=\frac{1}{2}$ Heisenberg antiferromagnetic in a magnetic field. The Hamiltonian is given by

$$\mathcal{H}=2J\sum_{l=1}^{N}\vec{S}_l\cdot\vec{S}_{l+1}-g\mu_B B\sum_{l=1}^{N}S_l^z \quad (J>0) \ . \tag{4.1}$$

We apply periodic boundary conditions $\vec{S}_{N+1}\equiv\vec{S}_1$. In order to simplify the formulas, dimensionless variables are introduced for frequency, energy, temperature, and magnetic field:

$$\tilde{\omega}\equiv\hbar\omega/2J, \quad \tilde{\epsilon}\equiv\epsilon/2J, \quad \tilde{T}\equiv k_BT/2J, \quad \tilde{H}\equiv g\mu_BB/2J \ . \tag{4.2}$$

In our calculations we make use of the following symmetries of the Hamiltonian (4.1):

(i) $\mathcal{H}$ is invariant with respect to lattice translations. Therefore each eigenstate can be labeled by a wave number $q=2\pi n/N$, $n=0,\pm1,\pm2,\ldots,\pm(N/2-1)$, and $N/2$ ($N$ assumed even).

(ii) $\mathcal{H}$ is invariant under rotations around the $z$ axis. This allows the introduction of the quantum number $S_T^z$, the $z$ component of the total spin.

(iii) $\mathcal{H}$ also commutes with $S_T$, the operator for the square of the total spin with eigenvalues $S_T(S_T+1)$. Thus $S_T$ is an additional quantum number.

Once the eigenvalues $E_\lambda$ and eigenfunctions $|\lambda\rangle$ are known, the Fourier transforms of the time-dependent pair-correlation functions can be evaluated as follows:

$$S^{\mu\nu}(q,\tilde{\omega})=N^{-1}\sum_{l,R}e^{iqR}\int_{-\infty}^{+\infty}dt\,\langle\delta S_l^\mu(t)\delta S_{l+R}^\nu(0)\rangle e^{i\omega t}$$

$$=\frac{2\pi}{Z}\sum_{\lambda\lambda'}e^{-\beta E_\lambda}\langle\lambda|S^\mu(q)|\lambda'\rangle\langle\lambda'|S^\nu(-q)|\lambda\rangle\delta(\tilde{\omega}+\tilde{E}_\lambda-\tilde{E}_{\lambda'})-2\pi\delta(\tilde{\omega})\langle S^\mu(q)\rangle\langle S^\nu(-q)\rangle \ . \tag{4.3}$$

Here $Z$ is the partition function, and

$$S^\mu(q)=N^{-1/2}\sum_l e^{-iql}S_l^\mu, \quad \mu=x,y,z \ . \tag{4.4}$$

We have introduced the operators $\delta S_l^\mu=S_l^\mu-\langle S_l^\mu\rangle$ which characterize the fluctuating parts of the spin components. Because of the symmetry properties of $\mathcal{H}$, $\langle S^\mu(q)\rangle\neq0$ only for $\mu=z$, $q=0$, and $\tilde{H}\neq0$. Therefore, the autocorrelation functions, in which we are interested here, read

$$F^{\mu\nu}(\tilde{\omega})=N^{-1}\sum_q S^{\mu\nu}(q_1\tilde{\omega})=\frac{2\pi}{ZN}\sum_{\lambda\lambda'q}e^{-\beta E_\lambda}\langle\lambda|S^\mu(q)|\lambda'\rangle\langle\lambda'|S^\nu(-q)|\lambda\rangle\delta(\tilde{\omega}+\tilde{E}_\lambda-\tilde{E}_{\lambda'})-2\pi\sigma^2\delta_{\mu z}\delta_{\nu z}\delta(\tilde{\omega}) \ , \tag{4.5}$$

where

$$\sigma \equiv N^{-1} \sum_{l=1}^{N} \langle S_l^z \rangle, \quad 0 \leq \sigma \leq \tfrac{1}{2} \tag{4.6}$$

is the magnetization. Instead of $F^{xx}$ and $F^{yy}$ it is more convenient to evaluate $F^{+-}$ and $F^{-+}$ using

$$S^{\pm}(q) = S^x(q) \pm iS^y(q) \ . \tag{4.7}$$

The use of selection rules which result from the symmetry properties (i) to (iii) of the Hamiltonian (4.1) facilitates greatly the determination of the nonvanishing matrix elements in Eqs. (4.3) and (4.5).[13,14,21]

Our aim is to calculate the temperature and field dependence of the dynamical autocorrelation functions $F^{\mu\nu}(\tilde{\omega})$ Eq. (4.5) for the Hamiltonian (4.1) in the limit $\tilde{\omega} \to 0$. For this purpose we use three different methods: (i) analytic (partly exact) calculations for $T = 0$; (ii) numerical finite-chain calculations for $T > 0$; and (iii) approximate analytic calculations for $T > 0$.

### A. Analytic calculations for $\tilde{T} = 0$ and $\tilde{H} = 0$

Using selection rules, finite-chain calculations and exact calculations in the Bethe formalism we have derived an approximate analytic expression for $S^{\mu\nu}(q, \tilde{\omega})$ at $\tilde{T} = 0$ and $\tilde{H} = 0$ (Refs. 12 and 14);

$$S^{\mu\nu}(q, \tilde{\omega}) = \frac{A}{[\tilde{\omega}^2 - \tilde{\epsilon}_1^2(q)]^{1/2}} \Theta(\tilde{\omega} - \tilde{\epsilon}_1(q)) \Theta(\tilde{\epsilon}_2(q) - \tilde{\omega}) \delta_{\mu\nu} \ . \tag{4.8}$$

This result takes into account excitations from the singlet ($S_T = 0$) ground state to the triplet ($S_T = 1$) spin-wave continuum with the lower boundary

$$\tilde{\epsilon}_1(q) = \tfrac{1}{2}\pi |\sin q| \tag{4.9}$$

and the upper boundary

$$\tilde{\epsilon}_2(q) = \pi |\sin q/2| \ . \tag{4.10}$$

Obviously, for $\tilde{H} = 0$, the two transverse components $S^{xx} = S^{yy}$ are equal to the longitudinal component $S^{zz}$. The autocorrelation function is immediately found by integration over $q$

$$F^{\mu\mu}(\tilde{\omega}) \equiv \int_{-\pi}^{+\pi} \frac{dq}{2\pi} S^{\mu\mu}(q, \tilde{\omega}) \ , \tag{4.11}$$

yielding a combination of elliptic integrals. It has a logarithmic divergence for $\tilde{\omega} = \pi/2$

$$F^{\mu\mu}(\tilde{\omega}) \sim |\ln|1 - 2\tilde{\omega}/\pi||, \quad \tilde{\omega} \sim \pi/2 \ . \tag{4.12}$$

In the zero-frequency limit it behaves as

$$F^{\mu\mu}(\tilde{\omega}) = A/\pi + O(\tilde{\omega}) \ . \tag{4.13}$$

The constant $A$ can be determined by various sum rules,[14] e.g., by the obvious requirement

$$\int_{-\infty}^{+\infty} \frac{d\tilde{\omega}}{2\pi} F^{\mu\mu}(\tilde{\omega}) = \langle (S_l^{\mu})^2 \rangle = \tfrac{1}{4}, \quad \mu = x,y,z \ . \tag{4.14}$$

This yields $A = \pi^2/8G \approx 1.35$ where $G \approx 0.916$ is Catalan's constant. In Fig. 5 we show this zero-temperature result for the autocorrelation function together with finite-chain results for various nonzero temperatures including $\tilde{T} = \infty$ (see Sec. IV D). An important feature of our result is that $F^{\mu\mu}(\tilde{\omega} = 0)$ is finite at $\tilde{T} = 0$. This is in contrast to the classical spin-wave result which predicts $F^{\mu\mu}(0) \propto T^{-1}$.[22] In Ref. 5 $F^{\mu\mu}(0)$ was calculated for the quantum chain, assuming the low-temperature dynamics to be governed by a single branch of noninteracting sharp spin waves. This assumption leads directly to the conclusion that $F^{\mu\mu}(0)$ is proportional to the static correlation function at $q = \pi$, a quantity which diverges for $T \to 0$. However, our calculations show that, since the low-temperature dynamics is governed by a two-parameter continuum of excitations, the autocorrelation function at $\tilde{\omega} = 0$ stays finite even though the static correlation function diverges at $q = \pi$.[12] The zero-frequency behavior at $\tilde{T} \neq 0$ is discussed below (Secs. IV D and IV E).

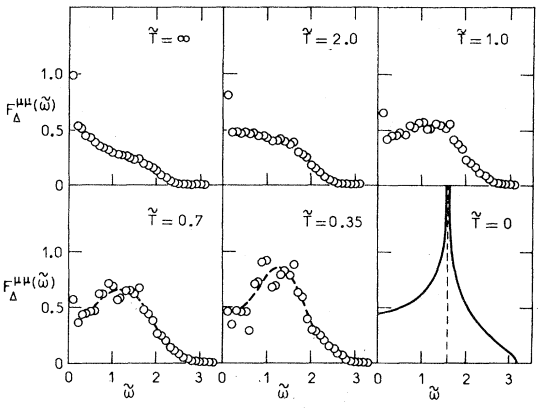


FIG. 5. Frequency dependence of the autocorrelation function for $\tilde{H} = 0$ at various temperatures. The circles represent finite-chain results for $F_{\Delta}^{\mu\mu}(\tilde{\omega})$, obtained by averaging results for $N = 9$ and $N = 10$ in order to account for an even-odd effect at small $\tilde{\omega}$, and by using an interval width $\Delta = 0.4$. The dashed lines are guides to the eye. The solid line for $\tilde{T} = 0$ represents the analytic result for $F^{\mu\mu}(\tilde{\omega})$ of Sec. II A.

### B. Exact results for $\tilde{T} = 0$ and $\tilde{H} > \tilde{H}_c$

In the presence of a uniform magnetic field $\tilde{H}$ parallel to the $z$ axis, the longitudinal component $F^{zz}$ and the transverse components $F^{xx} = F^{yy}$ have to be treated separately. For fields higher than the critical field ($\tilde{H} > \tilde{H}_c = 2$) the ground state $|G\rangle$ of the sys-

tem with energy $\tilde{E}_G$ is ferromagnetic, i.e., it has all spins lined up parallel to the field. It is easily shown that in this case the only excited states which can contribute to the transverse correlation function $S^{xx}(q,\tilde{\omega})=\frac{1}{4}[S^{+-}(q,\tilde{\omega})+S^{-+}(q,\tilde{\omega})]$ are the ferromagnetic spin waves $|k\rangle$. They form a single branch with energy

$$\tilde{E}_k=E_G+(\tilde{H}-\tilde{H}_c)+1+\cos k \quad . \tag{4.15}$$

Therefore, the dynamic correlation function can be written in the simple form

$$S^{xx}(q,\tilde{\omega})=\sum_k M_k(q)\delta(\tilde{\omega}+E_G=E_k) \quad . \tag{4.16}$$

The corresponding matrix elements can be evaluated exactly

$$M_k(q)\equiv\tfrac{1}{2}\pi|\langle G|S^+(q)|k\rangle|^2=\tfrac{1}{2}\pi\delta_{k,q} \quad . \tag{4.17}$$

Thus

$$S^{xx}(q,\tilde{\omega})=\tfrac{1}{2}\pi\delta(\tilde{\omega}-\tilde{H}+1-\cos q) \quad . \tag{4.18}$$

Integration over the Brillouin zone yields

$$F^{xx}(\tilde{\omega})=\frac{1/2}{[1-(\tilde{\omega}-\tilde{H}+1)^2]^{1/2}} \times\Theta(\tilde{\omega}-\tilde{H}+2)\Theta(\tilde{H}-\tilde{\omega}) \quad . \tag{4.19}$$

$F^{xx}(\tilde{\omega})$ vanishes outside the interval $\tilde{H}-2\leq\tilde{\omega}\leq\tilde{H}$ and is finite inside except at both boundaries where it has a square-root divergence. In contrast to the transverse spin waves there are no longitudinal fluctuations above the critical field, because there are no nonzero off-diagonal matrix elements of the kind $\langle\lambda|S^z(q)|G\rangle$. Thus

$$F^{zz}(\tilde{\omega})\equiv 0, \quad \tilde{H}>\tilde{H}_c \quad . \tag{4.20}$$

### C. Approximate results for $\tilde{T}=0$ and $0\leq\tilde{H}\leq\tilde{H}_c$

Finite-chain calculations and approximate analytic calculations[12,14] show that both $F^{xx}(\tilde{\omega})$ and $F^{zz}(\tilde{\omega})$ contain significant contributions from several continua of states, revealing therefore a complex behavior. However, these calculations suggest that the dominant contribution to $F^{xx}(\tilde{\omega}\approx 0)$ comes from excitations near $q=\pi$, as is also the case for $\tilde{H}=0$ and $\tilde{H}=\tilde{H}_c$. Bethe's formalism allows for an approximate calculation of the lower boundary of that spin-wave continuum which contributes to $F^{xx}(\tilde{\omega})$ at small $\tilde{\omega}$ (Refs. 14 and 30):

$$\tilde{\epsilon}_L(q)=2D|\cos q/2\sin(q/2-\pi\sigma)| \quad , \tag{4.21}$$

where the amplitude is given by $D=\pi/2+(\tilde{H}/2)\times(1-\pi/2)$. $\sigma$ is the magnetization which reads in this approximation

$$\sigma=\frac{1}{\pi}\arcsin\frac{1}{1-\pi/2+\pi/\tilde{H}} \quad . \tag{4.22}$$

Assuming that the spectral weight of $S^{xx}(q,\tilde{\omega})$ for $\tilde{\omega}$ above $\tilde{\epsilon}_L(q\approx\pi)$ still has a square-root behavior as in Eq. (4.8), $S^{xx}(q,\tilde{\omega})\propto[\tilde{\omega}^2-\tilde{\epsilon}_L^2(q)]^{-1/2}$, the $q$ integration can be performed. In the low-frequency limit it yields

$$F^{xx}(0^+)=\frac{A}{(4D^2-\tilde{H}^2)^{1/2}} \quad . \tag{4.23}$$

Note that this result takes into account not only the lowest branch $\tilde{\epsilon}_L(q)$ but also the continuum which lies above this lower threshold. At $\tilde{H}=0$ Eq. (4.13) is recovered and at $\tilde{H}=\tilde{H}_c^-$, $F^{xx}(0^+)$ diverges in consistency with Eq. (4.19). Figure 6 shows the result [Eq. (4.23)] for the $\tilde{T}=0$ field dependence of $F^{xx}(0^+)$ together with finite-chain results for various nonzero temperatures including $\tilde{T}=\infty$ (see Sec. IV D). Essentially the same behavior of $F^{xx}(\tilde{\omega})$ for $\tilde{\omega}\to 0$ as in Eq. (4.23), but with a somewhat smaller normalizing constant $A$ and a slightly different dependence on $\tilde{H}$ has been found by calculating $F^{xx}(\tilde{\omega})$ for the $XY$ chain and using the Bulaevskii approximation for the Heisenberg model.[8]

In contrast to $F^{xx}$ the behavior of $F^{zz}(\tilde{\omega}\approx 0)$ in intermediate fields is not quite clear for $\tilde{T}=0$. Quantitative results are restricted to the limiting cases $\tilde{H}=0$ where Eq. (4.13) is valid and, of course, $\tilde{H}>\tilde{H}_c$ where $F^{zz}(\tilde{\omega})\equiv 0$. Actually an exact solution of the longitudinal $\tilde{T}=0$ dynamics is available for $\tilde{H}=\tilde{H}_c^-$: in a field range of order $1/N^2$ below $\tilde{H}_c$ the ground state of the system is the lowest ferromagnetic spin wave $|\pi\rangle$ with energy $\tilde{E}_\pi=\tilde{E}_G^-$. Selection rules tell us that the only excited states which contribute to $S^{zz}(q,\tilde{\omega})$ are the ferromagnetic spin waves $|k\rangle$ with $k\neq\pi$. Therefore we can write

$$S^{zz}(q,\tilde{\omega})=\sum_{k\neq\pi} M_k(q)\delta(\tilde{\omega}+\tilde{E}_\pi-\tilde{E}_k) \tag{4.24}$$

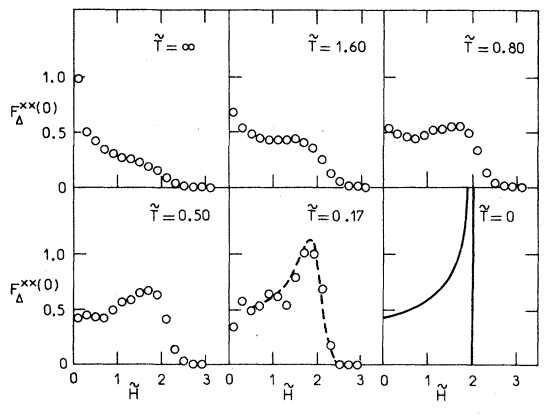


FIG. 6. Field dependence of the low-frequency transverse autocorrelation function at various temperatures. The circles represent finite-chain results for $F_\Delta^{xx}(0)$ ($N=8$, $\Delta=0.4$). The dashed line is a guide to the eye. The solid line for $\tilde{T}=0$ represents the analytic result [Eq. (4.23)] for $F^{xx}(0^+)$.

and evaluate the corresponding matrix elements

$$M_k(q) \equiv 2\pi |\langle \pi | S^z(q) | k \rangle|^2 = (2\pi/N)\delta_{q,k-\pi} \quad . \tag{4.25}$$

Thus, for $\tilde{H} = \tilde{H}_c^-$ we have

$$S^{zz}(q_1\tilde{\omega}) = (2\pi/N)\delta(\tilde{\omega} - 1 + \cos q) \quad , \tag{4.26}$$

which yields (for small $\tilde{\omega}$)

$$F^{zz}(\tilde{\omega}) = \frac{2}{N}\frac{1}{\sqrt{2\tilde{\omega}}} \tag{4.27}$$

in the limit of large $N$. We thus obtain an $\tilde{\omega}^{-1/2}$ divergence with a coefficient which vanishes in the thermodynamic limit. Unfortunately, this result covers only the limit $\lim_{N\to\infty} F^{zz}(\tilde{\omega}, \tilde{H}_c - \tilde{H} = 0(N^{-2}))$ but not the limit $\lim_{\tilde{H}\to\tilde{H}_c^-} \lim_{N\to\infty} F^{zz}(\tilde{\omega})$.

### D. Finite-chain calculations

This method is particularly valuable for nonzero temperatures, since most of the analytic approaches which are efficient either at $\tilde{T} = 0$ or $\tilde{T} = \infty$ cannot easily be generalized to arbitrary $\tilde{T}$, and the treatments applicable at arbitrary $\tilde{T}$ usually do not provide reliable results except for some special choice of the parameters (see, e.g., Sec. IV E). Finite-chain calculations for dynamic quantities were first performed by Richards and Carboni.[19,20] The first step of this approach is the numerical diagonalization of the Hamiltonian (4.1) in the Hilbert space of dimension $2^N$, where use is made of the symmetries (i) to (iii) described at the beginning of this section. Dynamic quantities like $S^{\mu\nu}(q, \tilde{\omega})$ and $F^{\mu\nu}(\tilde{\omega})$ are then evaluated directly according to Eqs. (4.3) and (4.5), respectively.

The finite-chain result for the frequency dependence of $F^{\mu\mu}(\tilde{\omega})$ is actually a set of $\delta$ functions. In order to interpret such results and to compare them with experiments or other theories we need a smoothed quantity which converges faster towards the thermodynamic limit. For this purpose we smooth any dynamic quantity $\psi(\tilde{\omega})$ from finite-chain calculations by an integral operation which removes the $\delta$ singularities

$$\psi_\Delta(\tilde{\omega}) = \frac{1}{\Delta}\int_{\tilde{\omega}-\Delta/2}^{\tilde{\omega}+\Delta/2} d\tilde{\omega}'\psi(\tilde{\omega}') \quad . \tag{4.28}$$

Finite-chain results for $\tilde{T} > 0$ in this paper always refer to Eq. (4.28). The interval width $\Delta$ has to be chosen empirically: large enough in order that finite-size effects are more or less smoothed out, but small enough that the physical structure is not smeared out. Figure 5 shows the frequency dependence of $F^{\mu\mu}(\tilde{\omega})$ at $\tilde{H} = 0$ obtained by finite-chain calculations for $N = 9$ and $N = 10$. With $\Delta$ fixed at 0.4 the results converge well to a smooth curve for elevated temperatures ($\tilde{T} \gtrsim 1.0$). At lower $\tilde{T}$ the number of appreciably populated states is significantly reduced and finite-size effects become more and more pronounced. Nevertheless the physical structure is still clearly observable at $\tilde{T}$ as low as 0.35. The finite-size effects could be further suppressed by a larger $\Delta$, but only at the cost of resolution. A careful study yields $\Delta = 0.4$ as an optimal choice for our purpose.

The result for $\tilde{T} = \infty$ reflects diffusive behavior with a sharp cusp at $\tilde{\omega} = 0$ and a broad shoulder at $\tilde{\omega} \approx \pi/2$. This is in agreement with an analytic calculation which expresses the autocorrelation function in terms of a "diffusivity" $D(q, \tilde{\omega})$ and assumes a two-parameter Gaussian for $D(q, \tilde{\omega})$.[31] The cusp in $F_\Delta^{\mu\mu}(\tilde{\omega})$ at $\tilde{\omega} = 0$ reflects the divergence of $F^{\mu\mu}(\tilde{\omega})$ for $\tilde{\omega} \to 0$ resulting from a one-dimensional density-of-states effect (see Sec. IV E). As the temperature is lowered the diffusive cusp diminishes only slowly, and the shoulder develops into a peak at $\tilde{\omega} = \pi/2$. This peak becomes higher and sharper until at $\tilde{T} = 0$ it transforms into a logarithmic divergence.

In connection with the $T_1$ measurements of Sec. III we are, of course, most interested in the field dependence of $F^{xx}(\tilde{\omega})$ and $F^{zz}(\tilde{\omega})$ at small $\tilde{\omega}$. We again use Eq. (4.28) for the presentation of finite-chain results. The $\tilde{H}$ dependence of $F^{+-}(0)$ and $F^{-+}(0)$ in Eq. (4.5) is introduced by Zeeman terms $\tilde{E}_\lambda^{ZE} = -\tilde{H}S_T^z(\lambda)$ in the energy eigenvalues. This effects $F^{xx}$ in two ways: (i) by the $\tilde{H}$ dependence of the statistical factors $Z^{-1}\exp(-\beta E_\lambda)$ which remains very smooth down to $\tilde{T} \approx 0.1$; and (ii) by additive terms $-\tilde{\omega}_e(+\tilde{\omega}_e)$ in the arguments of the $\delta$ functions of $F^{+-}$ ($F^{-+}$), where $\tilde{\omega}_e = \tilde{H}$ is the electronic Larmor frequency. In particular at $\tilde{T} = \infty$ we have[32]

$$F^{xx}(\tilde{\omega}_e, \tilde{H} = 0) = F^{xx}(\tilde{\omega} = 0, \tilde{H}) \quad . \tag{4.29}$$

Thus, for the field dependence of $F_\Delta^{xx}(0)$ we are faced with essentially the same finite-size effects as for its frequency dependence. However, in this case convergence is maintained (with the same $\Delta$) down to lower temperatures ($T \approx 0.2$). This is illustrated in Fig. 6. The result for $\tilde{T} = \infty$ reflects the frequency dependence in Fig. 5 according to Eq. (4.29). As $T$ is lowered the shoulder at $\tilde{H} \approx \pi/2$ again develops into a peak. In contrast to the $\tilde{\omega}$ peak of Fig. 5 this peak moves slightly to the right approaching $\tilde{H}_c = 2$ and becomes higher without losing its asymmetry until it recovers the $\tilde{T} = 0$ limiting behavior with a square-root divergence at $\tilde{H}_c^-$ and a cutoff for $\tilde{H} > \tilde{H}_c$.

The finite-chain results for $F_\Delta^{zz}(0)$ are found to be of the form $\alpha(\Delta)f(\tilde{H}, \tilde{T})$ where $\alpha(\Delta)$ shows a strong dependence on the interval width $\Delta$, but $f(\tilde{H}, \tilde{T})$ is only weakly $\Delta$ dependent for $\Delta \lesssim 0.2$. This behavior reflects the expected logarithmic divergence of $F^{zz}(\tilde{\omega})$ for $\tilde{\omega} \to 0$ due to one-dimensional density-of-states effects (see Sec. IV E). The $\tilde{H}$ dependence of $F_\Delta^{zz}(0)$ is much smoother than that of $F_\Delta^{xx}(0)$ owing to the fact that the Zeeman terms of $\tilde{E}_\lambda$ and $\tilde{E}_{\lambda'}$ cancel each other in the $\delta$ functions of

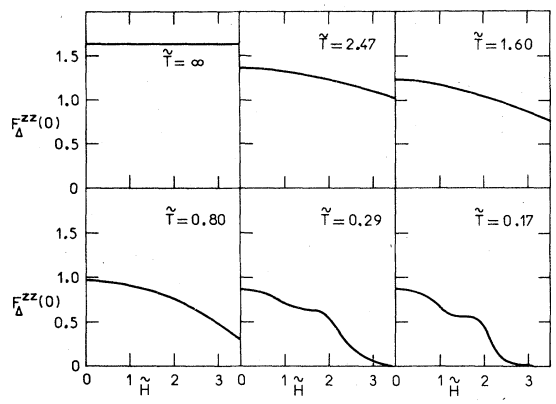


FIG. 7. Field dependence of the low-frequency longitudinal autocorrelation function at various temperatures. Finite-chain results for $F_\Delta^{zz}(0)$, obtained by averaging the results for $N=9$ and $N=10$ in order to account for an even-odd effect. Here $\Delta=0.2$ is used.

Eq. (4.5), leaving therefore the statistical factors $Z^{-1}\exp(-\beta\tilde{E}_\lambda)$ as the only $\tilde{H}$-dependent quantity in Eq. (4.5). In particular at $\tilde{T}=\infty$ $F^{zz}(\tilde{\omega})$ is no longer field dependent. At very low temperatures ($T\lesssim 0.1$), however, when the critical behavior at $\tilde{H}=\tilde{H}_c=2$ becomes important, the finite-chain results may no longer be reliable. Figure 7 shows the field dependence of $F_\Delta^{zz}(0)$ for various temperatures. The results are so normalized that they agree for the lowest temperature $\tilde{T}=0.17$ with the analytic result [Eq. (4.13)] for $\tilde{T}=0$. At $\tilde{T}=\infty$ the result is large [owing to the diffusive peak of $F^{\mu\mu}(\tilde{\omega})$ in Fig. 5] and field independent. As $\tilde{T}$ is lowered, the field dependence sets in very slowly. In contrast to $F^{xx}$, critical effects at $\tilde{H}=\tilde{H}_c$ become visible only below $\tilde{T}\approx 0.5$. There is no evidence for the development of a divergence at $\tilde{H}=\tilde{H}_c$ in the low-temperature limit. This is not surprising since critical fluctuations of an antiferromagnet at the critical field are expected to be exclusively transverse in character. We are not sure whether the plateau which develops for $\tilde{H}\lesssim\tilde{H}_c$ is real or due to a finite-size effect. It is interesting to note, however, that the corresponding curves for $F^{zz}(\tilde{\omega}\approx 0)$ of the $XY$ model[9] show a broad maximum near the critical field. At $\tilde{T}=0$ we have the analytic result for $\tilde{H}=0$, and we know that $F^{zz}(0)$ vanishes for $\tilde{H}>\tilde{H}_c$. The finite-chain results indicate that $F^{zz}(0)$ varies smoothly for $\tilde{H}<\tilde{H}_c$ and that at $\tilde{H}=\tilde{H}_c$ it probably drops from some finite value to zero.

### E. Calculations in an effective $XY$ approximation

A model which is more amenable to exact solutions than the HB AF [Eq. (4.1)] is the $XY$ model with Hamiltonian

$$\mathcal{H}_{XY}=2J\sum_{l=1}^{N}(S_l^xS_{l+1}^x+S_l^yS_{l+1}^y)-g\mu_BB\sum_{l=1}^{N}S_l^z \quad . \tag{4.30}$$

Generally, this model is not a good approximation to the HB AF. However, above the critical field, which is $\tilde{H}_c=1$ for the $XY$ model and $\tilde{H}_c=2$ for the HB AF, both models have the same ground state and identical excited states dominating the $\tilde{T}=0$ dynamics. These common eigenstates have been discussed in Sec. IV B. The similarity of the two models above $\tilde{H}_c$ is further demonstrated in the fermion representation. As is well known, the $XY$ model can be mapped into a system of noninteracting fermions[33] which allows for an exact treatment in many aspects. Correspondingly, the HB AF is transformed into a system of interacting fermions, lacking an exact solution. An obvious approximation introduced by Bulaevskii[34] is a self-consistent Hartree-Fock treatment, which transforms the HB AF into an effective $XY$ model whose parameters are solutions of two coupled integral equations. The transverse autocorrelation function at low frequencies could be obtained reliably in this approach.[8] But for higher frequencies and $\tilde{H}<\tilde{H}_c$ the dynamics of this effective $XY$ model is quite different from that of the true HB AF, even at $\tilde{T}=0$.[14] For $\tilde{H}>\tilde{H}_c$, however, the Bulaevskii approach can account exactly for the fermion interaction in the HB AF at $\tilde{T}=0$. It reproduces in particular the correct value for the critical field ($\tilde{H}_c=2$). Therefore, we can assume that for $\tilde{H}>\tilde{H}_c$ and low $\tilde{T}$ the dynamics of the HB AF is well reproduced by the $XY$ dynamics. Niemeijer has obtained an exact formula for the longitudinal two-spin correlation function $\langle S_l^z(t)S_{l+R}^z(0)\rangle$ of the $XY$ model for arbitrary $\tilde{T}$ and $\tilde{H}$.[9] A straightforward calculation yields the corresponding Fourier transformed autocorrelation function

$$F^{zz}(\tilde{\omega})=\frac{1}{2\pi}\int_0^1 dx\frac{[1+\tanh\frac{1}{2}B(x-\tilde{H})][1-\tanh\frac{1}{2}B(x-\tilde{\omega}-\tilde{H})]}{[(1-x)(1+x)(1-\tilde{\omega}+x)(1+\tilde{\omega}-x)]^{1/2}}$$
$$+\frac{1}{2\pi}\int_{\tilde{\omega}}^1 dx\frac{[1+\tanh\frac{1}{2}B(x+\tilde{H})][1-\tanh\frac{1}{2}B(x-\tilde{\omega}+\tilde{H})]}{[(1-x)(1+x)(1-\tilde{\omega}+x)(1+\tilde{\omega}-x)]^{1/2}} \quad (0\leq\tilde{\omega}\leq 1) \quad . \tag{4.31a}$$

The determination of Bulaevskii's parameters for the effective $XY$ model approximating the HB AF requires, in general, the solution of two coupled integral equations. A simple solution exists only for $\tilde{T}=0$,[34] but since we are interested mainly in the dynamics at the very low $\tilde{T}$, the $\tilde{T}=0$ values of the parameters are sufficient for our pur-

poses. The effect of the fermion interaction on Eq. (4.31) is then reduced to the replacement

$$\tilde{H} \rightarrow \tilde{H} - 1 \ , \tag{4.31b}$$

which accounts for the correct value of the critical field. Thus we are calculating two-fermion correlation functions for free fermions but use the Hartree-Fock energies for the single fermions.

Equation (4.31a) yields for $T \neq 0$ a logarithmic divergence of $F^{zz}(\tilde{\omega})$ for $\tilde{\omega} \rightarrow 0$ of the form

$$F^{zz}(\tilde{\omega}) \sim e^{-1/\tilde{T}} |\ln \tilde{\omega}| \ . \tag{4.32}$$

This divergence can be traced in the fermion representation to the thermal excitation of levels at the edge and the center of the Brillouin zone where the density of states diverges in one dimension as $(\epsilon - \epsilon_B)^{-1/2}$. Since this density-of-states effect should remain essentially unchanged by the interaction between the fermions, we expect the same type of singularity to occur also in the Heisenberg model. When integrated over an interval $\Delta$, it leads to a cusplike behavior $F^{zz}_{\Delta}(\tilde{\omega})$ at $\tilde{\omega} = 0$ and to a $\Delta$ dependence of $F^{zz}_{\Delta}(0)$ as discussed in Sec. IV D. In order to calculate the temperature and field dependence of $F^{zz}$ in the low-frequency limit, we either have to calculate $F^{zz}(\tilde{\omega})$ for some nonzero — albeit small — $\tilde{\omega}_0$, or we have to smooth $F^{zz}(\tilde{\omega})$ over some nonzero interval $\Delta$ as in Eq. (4.28). For a logarithmic singularity the temperature and field dependence is practically unaffected by the choice of $\tilde{\omega}_0$ or $\Delta$ in a suitable range, and only the scale depends strongly on $\tilde{\omega}_0$ or $\Delta$. Figure 8 compares the result of this effective $XY$ model with finite-chain results above the critical field at various $\tilde{T}$. The normalization is chosen such that the $XY$ result fits the finite-chain result at $\tilde{H} = \tilde{H}_c = 2$ at the lowest temperature $\tilde{T} = 0.17$. At this temperature, where the effective $XY$ model is most reliable, the agreement is excellent. Also the temperature dependence at $\tilde{H} = \tilde{H}_c$ is in satisfactory agreement. At higher temperatures, the field dependence still shows the same qualitative behavior, but clear deviations develop.

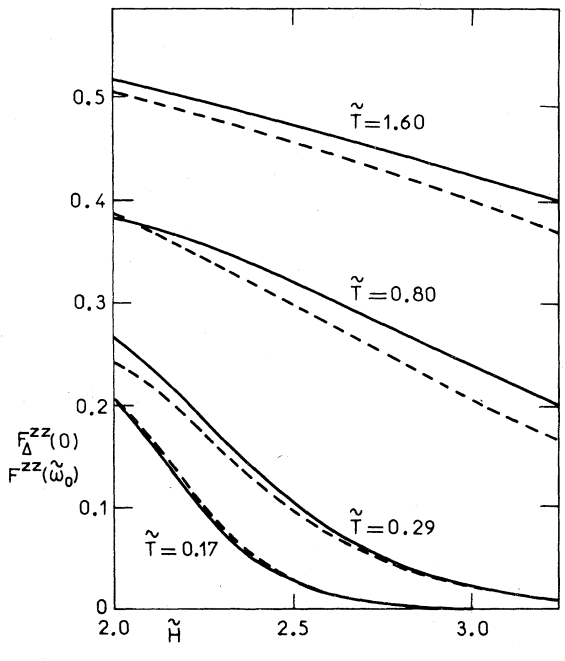


FIG. 8. Field dependence of $F^{zz}$ in the low-frequency limit for $\tilde{H} \geq \tilde{H}_c$ at various temperatures. The solid lines represent finite-chain results for $F^{zz}_{\Delta}(0)$ with $\Delta = 0.2$, obtained by averaging the results for $N = 9$ and $N = 10$. The dashed lines represent the effective $XY$ result [Eq. (4.31)] with $\tilde{\omega}_0 = 0.01$ and a normalization which fits the finite-chain result at $\tilde{H} = 2$ for the lowest temperature $\tilde{T} = 0.17$.

## V. EXPERIMENTAL RESULTS AND COMPARISON WITH THEORY

As discussed in Sec. III, experimental information on the field dependence of $\phi_0^+(\omega_n)$ can be obtained by measurements of $T_{1n}^{-1}$ at some special direction of the field. In Fig. 9 we show the data for $CuSeO_4 \cdot 5H_2O$ at three different temperatures. At 4.2 K which is high compared to the exchange interaction, we already find a characteristic decrease of the relaxation rate at the critical field $B_c = 4J/g\mu_B$ ($\tilde{H}_c = 2$). For temperatures comparable to the exchange (e.g., $T = 1.35$ K) a maximum just below $B_c$ begins to develop, which becomes more and more pronounced as $T$ is lowered, and the decrease above $B_c$ becomes very steep. The same features are observed in the data for $CuSO_4 \cdot 5H_2O$ shown in Fig. 10. Here we reach a significantly lower value of the reduced temperature $\tilde{T} = k_B T/2J$. Therefore, the characteristic behavior for low temperatures is even more pronounced. It was not possible to obtain reliable data for low fields, because there the different resonance lines overlap. In both Figs. 9 and 10 we compare the data with finite-chain results for $F^{xx}_{\Delta}(0)$ for the same reduced temperatures. The absolute value of the coefficient $b_{00}$ in Eq. (2.4) has been adjusted by fitting the theoretical predictions for $F^{xx}_{\Delta}(0)$ to the experimental values of $T_{1n}^{-1}$ at the lowest temperature. For $CuSO_4 \cdot 5H_2O$ we obtain a value for $b_{00}$ which agrees within experimental accuracy with the value calculated by using the point-dipolar model (2.6). For $CuSeO_4 \cdot 5H_2O$, on the other hand, this fit leads to a $b_{00}$ value which is roughly 20% too small. Figures 9 and 10 demonstrate that the different field dependence of $T_{1n}^{-1}$ at different temperatures is well reproduced by the finite-chain results, especially in view of the fact that the theoretical data contain only the single fit parameter $b_{00}$. For low temperatures the relaxation rate for $B > B_c$ is not reproduced

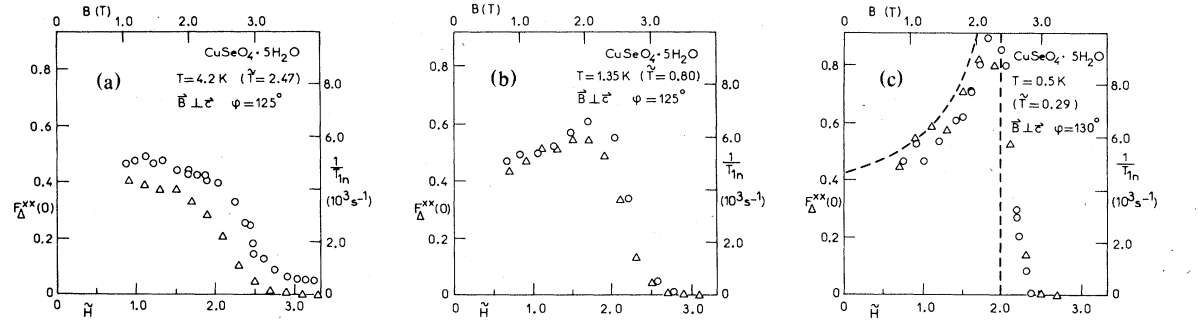


FIG. 9. (a)–(c) Experimental results (circles) for the field dependence of the relaxation rate of proton 3 in $CuSeO_4 \cdot 5H_2O$ at three different temperatures and for a field direction $\phi \approx 125°$, where the contribution of $\phi_0^+(\omega_n)$ is dominant. Comparison with finite-chain results (triangles) for the field dependence of $F_\Delta^{xx}(0)$ obtained by using $N=8$ and $\Delta=0.4$. The dashed line at $\tilde{T}=0.29$ indicates the theoretical prediction [Eq. (4.23)] in the low-temperature limit.

quantitatively due to the poor convergence of the finite-chain calculations in this region. The small deviations between theory and experiments for the higher temperatures can be attributed to small contributions of $\phi_p^z(\omega_n)$ and $\phi_0^z(\omega_n)$ to the relaxation rate. These deviations could have been expected in view of the results for the angular dependence of the relaxation rate, as discussed in Sec. III. In Figs. 9(c) and 10(c) we include the prediction based on the spin-wave continuum approach [Eq. (4.23)], which has a square-root divergence at $B_c$ followed by a cutoff above $B_c$. It is in excellent agreement with the data at the lowest reduced temperature $\tilde{T}=0.17$. Moreover, this critical behavior is already observable in the data for $\tilde{T}=0.29$ as well as in the low-$\tilde{T}$ finite-chain results. A similar zero-temperature result has been obtained in Ref. 8 by using Bulaevskii's approximation, and equally good agreement was found with the experimental data.

In Fig. 11 we present low-temperature experimental data for a different field direction, which reflect the field dependence of $\phi_0^z(\omega_n)$. The contribution of $\phi_0^+(\omega_n)$ at this angle, as determined from the previous results, has been subtracted; for comparison it is also shown in the figure. Clearly, the contribution of $\phi_0^+(\omega_n)$ to the relaxation rate is very small for $H \gtrsim 2.15$. Therefore, for these fields the inaccuracy in $\phi_0^z(\omega_n)$ due to the uncertainty in the $\phi_0^+(\omega_n)$ contribution is negligible compared to the experimental resolution of about 5%. For fields below $\tilde{H}=2$ the inaccuracy in $\phi_0^z(\omega_n)$ is much larger as a consequence of the large value of $\phi_0^+(\omega_n)$. Measurements of the

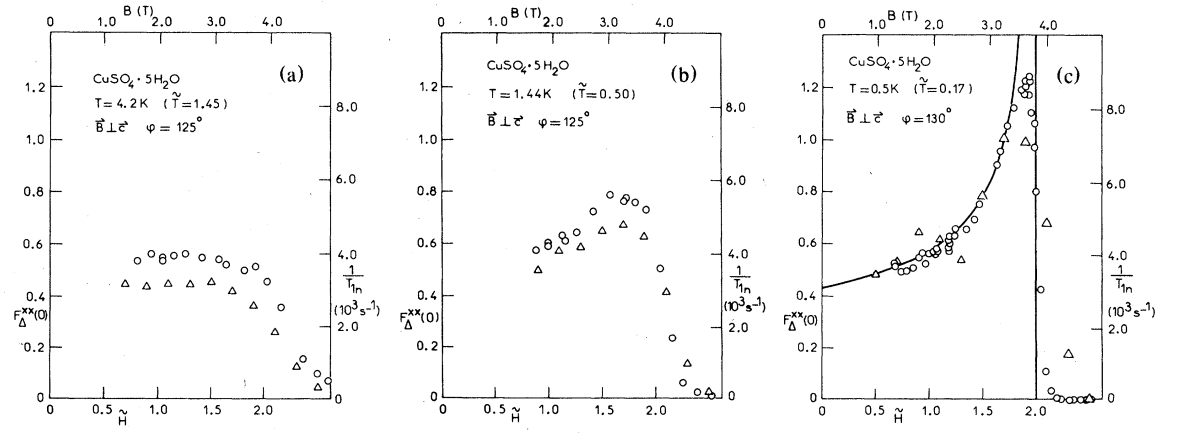


FIG. 10. (a)–(c) Experimental results (circles) for the field dependence of the relaxation rate of proton 3 in $CuSO_4 \cdot 5H_2O$ at three different temperatures and for a field direction $\phi \approx 125°$, where the contribution of $\phi_0^+(\omega_n)$ is dominant. Comparison with finite-chain results (triangles) for the field dependence of $F_\Delta^{xx}(0)$ is obtained by using $N=8$ and $\Delta=0.4$. The solid line for $\tilde{T}=0.17$ represents the analytical result [Eq. (4.23)] for $\tilde{T}=0$.

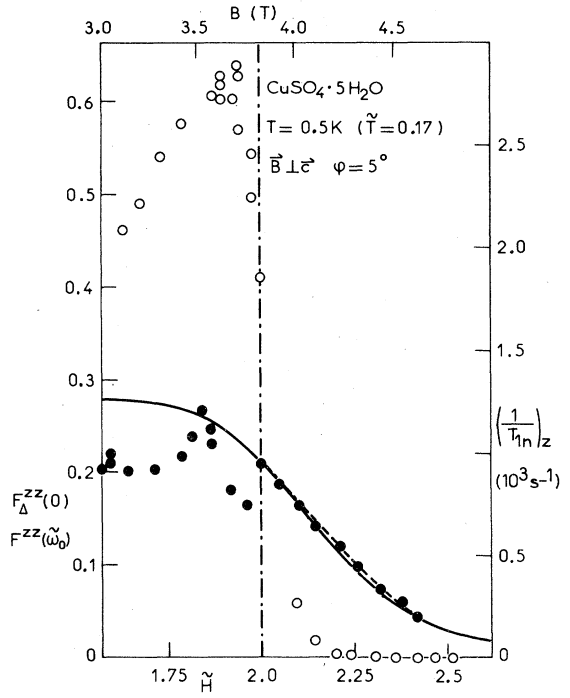


FIG. 11. Field dependence of the $\phi_0^z(\omega_n)$ contribution to the relaxation rate in $CuSO_4 \cdot 5H_2O$ for $\phi = 5°$ at $T = 0.5$ K and high magnetic fields (full circles). The $\phi_0^+(\omega_n)$ contribution for this field direction as determined from the measurements at $\phi = 125°$ has been subtracted from the measured relaxation rates. For comparison, this contribution is also shown (open circles). The solid line represents the finite-chain result for $F_\Delta^{zz}(0)$ ($N = 9$, 10; $\Delta = 0.2$) and the dashed line at $\tilde{H} \geq \tilde{H}_c$ the effective $XY$ results for $F^{zz}(\tilde{\omega}_0)(\tilde{\omega}_0 = 0.01)$, both at the same reduced temperature.

relaxation times of other protons, near the paramagnetic ion, show that for the results in Fig. 11 the contribution to the relaxation rate from the paramagnetic system is certainly less than 20 $s^{-1}$. Therefore this contribution has been neglected. The most important feature is the fact that above $B_c$ $\phi_0^z(\omega_n)$ decreases much more slowly than $\phi_0^+(\omega_n)$. The solid line represents the finite-chain results and the dashed line the effective $XY$ result for the field dependence of $F^{zz}(\tilde{\omega}_n)$ at the appropriate reduced temperature. Both approaches, discussed extensively in Sec. IV, yield excellent agreement with the data for $\tilde{H} \geq \tilde{H}_c$. Both curves have been scaled with respect to the data point at $\tilde{H} = \tilde{H}_c$. This normalization differs about 45% from what would be predicted by using the point dipolar model. The situation for higher $\tilde{T}$ and lower $\tilde{H}$ is not yet clear and requires further experimental and theoretical studies.

The striking difference between $F^{zz}(0)$ and $F^{xx}(0)$ above the critical field is best understood by looking at the eigenstates as in Sec. IV D. The slow decrease of $F^{zz}(0)$ with $\tilde{H}$ (for $\tilde{H} > \tilde{H}_c$) is obviously an effect of the statistical factor in Eq. (4.5) which, due to the Zeeman energy, suppresses gradually the population of the excited states and therefore their contribution to $F^{zz}(0)$. On the other hand, the pairs of states involved in matrix elements contributing to $F^{xx}$ are shifted by the field with respect to each other. For $\tilde{H} > \tilde{H}_c$, practically all pairs of states which contribute significantly to $F^{xx}$ have already crossed in energy with respect to each other and are no longer able to contribute to $F^{xx}(0)$, leading to a more or less abrupt decrease of $F^{xx}(0)$ at $\tilde{H} \approx \tilde{H}_c$. This effect is only weakly $T$ dependent; i.e., $F^{xx}(0) \approx 0$ at $\tilde{H} > \tilde{H}_c$ already for elevated temperatures.

The experimental results on CuNSal (Ref. 15) for $\phi_0^z(\omega_n)$ are more field dependent than ours at the same relative temperature (roughly a factor 2 in slope). The origin of this difference is not clear to us. They interpreted their data in a boson and fermion "picture" of the elementary excitations of the spin chain (based on approximate realizations of the Holstein-Primakoff and the Jordan-Wigner transformations, respectively). They found that the transverse fluctuations [our $F^{xx}(0)$] were well described in the fermion representation, whereas the data corresponding to $F^{zz}(0)$ were much better reproduced (for $\tilde{H} > \tilde{H}_c$) by a boson description. We emphasize that in our case the field dependence of $F^{zz}(0)$, for $\tilde{H} > \tilde{H}_c$, is very well given by our effective $XY$ approximation, i.e., by a calculation within the framework of the fermion representation of the $s = \frac{1}{2}$ spin system.

In conclusion we can state that the low-frequency dynamics of the $s = \frac{1}{2}$ antiferromagnetic Heisenberg chain in nonzero magnetic fields is understood in many aspects. The NMR $T_{1n}$ measurements have given detailed information about the characteristic features of the transverse autocorrelation function and some results for the longitudinal autocorrelation function. For comparison we have used finite-chain calculations for $T > 0$, analytic calculations for $T = 0$, as well as an effective $XY$ approach for nonzero $T$. It is found that for the chain lengths $N = 8$, 9, and 10 used in the present study, finite-size effects are not so serious even at relatively low temperatures, as to prevent a quantitative comparison with the NMR results. At very low temperatures, on the other hand, where the critical behavior near the saturation field becomes important, the NMR data for the transverse autocorrelations are better explained by the $T = 0$ analytical approach of Sec. IV C or by the theory of Ref. 8 based on the $XY$ model. The low-$T$ NMR data for the longitudinal autocorrelations at $\tilde{H} > \tilde{H}_c$ are perfectly reproduced by finite-chain results as well as by the results of a $T > 0$ effective $XY$ approach. Nevertheless, the longitudinal autocorrelations require further experimental and theoretical study.

## ACKNOWLEDGMENTS

The authors are indebted to Professor J. C. Bonner and to Professor H. W. Capel for valuable suggestions and for carefully reading the manuscript. One of us (G.M.) thanks the Kamerlingh Onnes Laboratorium for hospitality during his visit in Leiden. This work is supported by the Swiss National Foundation and is part of the research program of the Stichting voor Fundamenteel Onderzoek der Materie (FOM), which is financially supported by the Nederlandse Organisatie voor Zuiver Wetenschappelijk Onderzoek (ZWO).

[1]M. T. Hutchings, G. Shirane, R. J. Birgeneau, and S. L. Holt, Phys. Rev. B 5, 1999 (1972).
[2]Y. Endoh, G. Shirane, R. J. Birgeneau, P. M. Richards, and S. L. Holt, Phys. Rev. Lett. 32, 170 (1974).
[3]A. Lagendijk and E. Siegel, Solid State Commun. 20, 709 (1976).
[4]H. L. van Noort, Ph.D. thesis (Leiden, 1977) (unpublished).
[5]P. M. Richards and F. Borsa, Solid State Commun. 15, 135 (1974).
[6]J. P. Boucher, M. Ahmed Bakheit, M. Nechtschein, M. Villa, G. Bonera, and F. Borsa, Phys. Rev. B 13, 4098 (1976).
[7]I. U. Heilmann, G. Shirane, Y. Endoh, R. J. Birgeneau, and S. L. Holt, Phys. Rev. B 18, 3530 (1978).
[8]J. P. Groen, H. W. Capel, J. H. H. Perk, T. O. Klaassen, and N. J. Poulis, Physica (Utrecht) 97B, 126 (1979); J. P. Groen, T. O. Klaassen, and N. J. Poulis, Phys. Lett. 68A, 381 (1978).
[9]T. Niemeijer, Physica (Utrecht) 36, 377 (1967).
[10]S. Katsura, T. Horiguchi, and M. Suzuki, Physica (Utrecht) 46, 67 (1970).
[11]J. H. H. Perk and H. W. Capel, Physica (Utrecht) 89A, 265 (1977).
[12]G. Müller, H. Beck, and J. C. Bonner, Phys. Rev. Lett. 43, 75 (1979).
[13]G. Müller, H. Beck, and J. C. Bonner, J. Appl. Phys. 50, 7404 (1979).
[14]G. Müller, H. Thomas, H. Beck, and J. C. Bonner (unpublished).
[15]L. J. Azevedo, A. Narath, P. M. Richards, and Z. G. Soos, Phys. Rev. Lett. 43, 875 (1979).
[16]L. S. J. M. Henkens, K. M. Diederix, T. O. Klaassen, and N. J. Poulis, Physica (Utrecht) 83B, 147 (1976).
[17]J. C. Bonner and M. E. Fisher, Phys. Rev. 135, A640 (1964).
[18]H. W. J. Blöte, Physica (Utrecht) 79B, 427 (1975).
[19]F. Carboni and P. M. Richards, Phys. Rev. 177, 889 (1969).
[20]P. M. Richards and F. Carboni, Phys. Rev. B 5, 2014 (1972).
[21]G. Müller and H. Beck, J. Phys. C 11, 483 (1978).
[22]P. M. Richards, Phys. Rev. Lett. 28, 1646 (1972).
[23]S. Wittekoek, T. O. Klaassen, and N. J. Poulis, Physica (Utrecht) 39, 293 (1968).
[24]M. W. van Tol and N. J. Poulis, Physica (Utrecht) 69, 341 (1973).
[25]L. S. J. M. Henkens, T. O. Klaassen, and N. J. Poulis, Physica (Utrecht) 94B, 27 (1978).
[26]J. P. Groen, T. O. Klaassen, and N. J. Poulis, Phys. Lett. 68A, 381 (1978).
[27]T. Moriya, Prog. Theor. Phys. 16, 23 (1956).
[28]L. S. J. M. Henkens, M. W. van Tol. H. J. L. van der Valk, and N. J. Poulis, J. Phys. E 10, 719 (1977).
[29]G. E. Bacon and N. A. Curry, Proc. R. Soc. London Sect. A 226, 95 (1962).
[30]G. Müller, H. Beck, and J. C. Bonner, J. Magn. Magn. Mater. 15–18, 367 (1980).
[31]R. A. Tahir Kheli and D. G. Mc Fadden, Phys. Rev. 178, 800 (1969).
[32]S. M. Myers and A. Narath, Phys. Rev. Lett. 27, 641 (1971).
[33]E. H. Lieb, T. Schultz, and D. C. Mattis, Ann. Phys. (N.Y.) 16, 407 (1961).
[34]L. N. Bulaevskii, Sov. Phys. JETP 16, 685 (1963).